J Mater Sci: Mater Med (2008) 19:2437–2444
DOI 10.1007/s10856-008-3371-z

Pressureless sintering of dense hydroxyapatite–zirconia composites

Y. Nayak · R. P. Rana · S. K. Pratihar · S. Bhattacharyya

Received: 30 December 2006 / Accepted: 2 January 2008 / Published online: 25 January 2008

Abstract Hydroxyapatite (HA)–TZP (2.5 mol% Y_2O_3) containing 2, 5, 7.5 and 10 wt% TZP were prepared using calcium nitrate, diammonium hydrogen orthophosphate, zirconium oxychloride and yttrium nitrate. The composite powder was prepared by a reverse strike precipitation method at a pH of 10.5. The precipitates after aging and washing were calcined at 850°C to yield fine crystallites of HA and TZP. TEM study of the calcined powder revealed that while HA particles had both spherical and cuboidal morphology (~50–100 nm) the TZP particles were only of spherical nature (~50 nm). X-ray analysis showed that the calcined powder of all the four composition had only HA and t-ZrO_2. Uniaxially compacted samples were sintered in air in the temperature range 1,150–1,250°C. High sintered density (>95% of theoretical) was obtained for composites containing 2 and 5 wt% TZP, while it was 92% for 7.5 wt% and 90% for 10 wt% TZP compositions. X-ray analysis of sintered samples shows that with 2 wt% TZP, the retained phases were only HA and t-ZrO_2. However, for 5, 7.5 and 10 wt% TZP addition both TCP and $CaZrO_3$ were also observed along with HA and t-ZrO_2. Bending strength was measured by three point bending as well by diametral compression test. While in three point bending, the highest strength was 72 MPa, it was 35.5 MPa for diametral compression. The strength shows a decreasing trend at higher ZrO_2 content. SEM pictures show near uniform distribution of ZrO_2 in HA matrix. The reduction in sintered density at higher ZrO_2 content could be related to difference in the sintering behaviour of HA and ZrO_2.

Y. Nayak · R. P. Rana · S. K. Pratihar (✉) · S. Bhattacharyya
Department of Ceramic Engineering, National institute of Technology, Rourkela 769008, India
e-mail: skpratihar@nitrkl.ac.in

1 Introduction

Hydroxyapatite (HA) ceramics have widespread applicability in the biomedical field for repair or replacement of bone tissues. Owing to low strength and toughness of HA, its use is limited mainly to the non-load bearing components, e.g., small unloaded or low loaded implants, coating on metal implants and as bioactive filler as a powder or as a second phase in polymer based composites [1–3]. For load bearing applications, the research on the use of HA as bioactive filler in ceramic and metallic matrix composites did not succeed due to the deleterious reactions taking place between HA and the matrix phase [4–6]. However, the use of HA in load bearing parts can be explored provided the strength and toughness of HA can be increased [7]. Among many oxide reinforcements, ZrO_2 is an important one, which has been used to increase the strength and toughness of Al_2O_3, mullite, spinel and many other ceramic materials. High sintered density and ultra fine particles (in the nano range) will ensure retention of ZrO_2 mostly in tetragonal phase, which is expected to provide improved mechanical properties of the composites due to the transformation toughening effect of tetragonal ZrO_2. A number of approaches have been tried to prepare HA–ZrO_2 composites containing higher fraction of ZrO_2 (20–40 vol%) [8, 9] as well as there are some reports on the processing of HA–ZrO_2 composites containing low volume fraction (<20 vol%) ZrO_2 [10, 11]. These studies mostly concentrated on the densification behaviour of the composite and the stability of HA phase in the sintered HA–ZrO_2 composites. While high density HA could even be prepared by pressure less sintering in the temperature range 1,100–1,300°C [10–12], many of the HA–ZrO_2 composites did not densify properly in the above temperature range and the decomposition of HA to TCP was also observed in

many studies [12–15]. In fact, the decomposition of HA to TCP is accelerated at the higher sintering temperature (>1,300°C). With ZrO_2 addition, the decomposition temperature is further lowered (in the range 1,000–1,050°C) [16, 17]. Thus there is a need to control the decomposition of HA to TCP with ZrO_2 addition by controlling the powder characteristics during its preparation as well as by controlling the sintering parameters. The use of fine and highly reactive HA and ZrO_2 particles for preparing the composites also did not help in lowering the sintering temperature appreciably due the formation of hard agglomerates in fine and reactive powders [18, 19]. Therefore, even with these powders, densification at lower sintering temperature were obtained using either hot pressing/hot isostatic pressing [20–22] or spark plasma sintering [7, 23] or the use of additives (like CaF_2) which promote densification by altering the grain boundary characteristics [8], and inspite of using these advanced processing and consolidation techniques, the sintering temperature was usually not less than 1,000°C [7, 20, 22–29]. Most of the study on HA–ZrO_2 system concentrated on the densification behaviour and mechanical properties containing high volume fraction of ZrO_2 (20–40 vol% ZrO_2) although there are some reports on HA–ZrO_2 composites containing low volume fraction (≤20 vol%) ZrO_2 [11]. The study by Ahn et al. [11] discusses the effect of zirconia/YTZP reinforcing agent on the microstructure and mechanical properties of hot pressed hydroxyapatite-based nanocomposites (ZrO_2 1.5–15 wt%). In this study, high Vickers hardness (7.3 GPa) and bending strength (>200 MPa) was reported for HA–ZrO_2 composites for ZrO_2 addition up to 3 wt%. The study also pointed out that at very low volume percent addition of ZrO_2 (up to 3 wt%), the improvement in strength and hardness was significant However, since high density of the composites in this investigation was obtained by hot pressing at 1,000°C, which requires costly infrastructure and is therefore expensive.

Thus the present study aims to prepare HA–ZrO_2 composite containing uniform dispersion of ZrO_2 by reverse strike precipitation route and to achieve a high sintered density of these composites with out using any sintering additive and with minimum decomposition of HA to TCP by pressure less sintering. Thus the aim of the present study is much different from the earlier studies wherein high sintered densities of HA–ZrO_2 composites was obtained by Hot pressing or by Hot Isostatic Pressing or by Spark plasma sintering**.** These sintered composites will be characterized with respect to their strength, hardness and microstructure. The exact effect of ZrO_2 addition (both at low and high ZrO_2 loading) cannot be understood unless a systematic investigation in this system is carried out. But from the literature review, it appears that ZrO_2 probably plays a different role at low volume fraction addition (may act as a sintering aid) and at high volume fraction ZrO_2 addition (where its role may be dispersion strengthening).

2 Experimental

The hydroxyapatite–zirconia composite preparation consisted of the following steps:

(a) Preparation of nano TZP (2.5 mol% Y_2O_3) powder using precipitation method and
(b) Preparation of hydroxyapatite–zirconia composite (containing 2, 5, 7.5 and 10 wt% TZP and denoted as HZ2, HZ5, HZ7, HZ10, respectively) by reverse strike precipitation method (explained later).

The precursors used for TZP (2.5 mol% Y_2O_3) were $ZrOCl_2.8H_2O$ (Loba chemical, India) and Y_2O_3 (Indian Rare Earth Limited, India). Flow diagram of ZTP powder preparation was given in Fig. 1a. The concentration of $ZrOCl_2$ solution was 0.75 mol/l in which requisite amount of Y_2O_3 powder was dissolved. Precipitation was carried

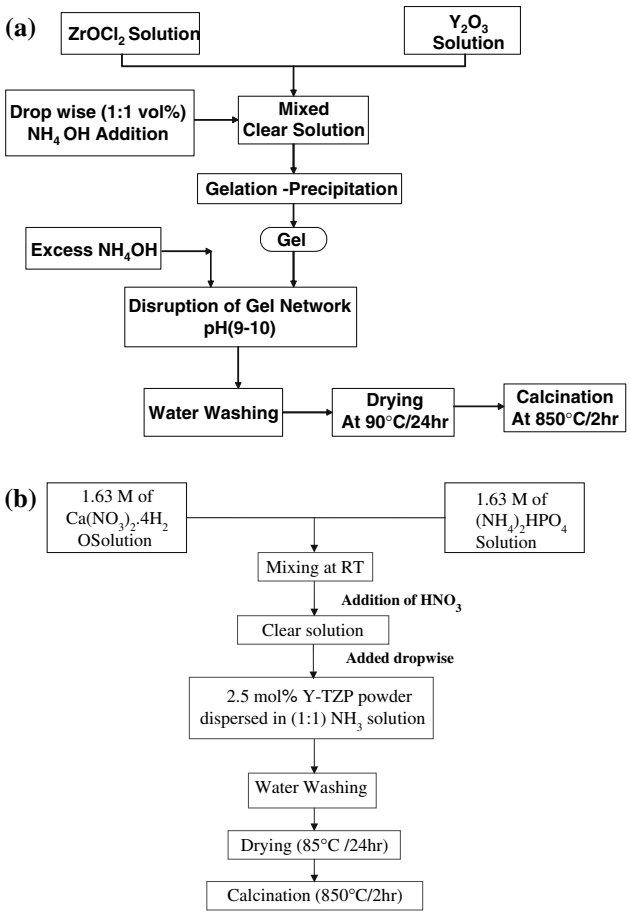

Fig. 1 Flow Diagram for Synthesis of (**a**) 2.5Y-TZP; (**b**) HA–(2, 5, 7.5, 10 wt%) TZP

out using NH_4OH (1:1) solution. The precipitates were washed to remove chloride ions followed by drying and calcination at 850°C/2 h. The process flow diagram for HA–TZP composites is shown in Fig. 1b. In this process, equimolar solution (1.63 mol/l) of both $Ca(NO_3)_2 \cdot 2H_2O$ (Oster Chemical, India) and $(NH_4)_2HPO_4$ (Nice Chemical, India) were mixed together. Sometimes, a few drops of HNO_3 is added to get a clear solution. This clear solution was dropwise added to a beaker containing calcined TZP powder dispersed in (1:1) NH_4OH solution. This precipitation process, is thus different from the normal precipitation process, wherein the precipitating agent (e.g., NH_4OH) is added to the mixed cation solution. This precipitation process as discussed above and adopted in this investigation is termed as reverse strike precipitation process. The as precipitated powder having varying proportion of ZrO_2 were subjected to hot water and propanol washing to remove the extraneous ions and excess hydroxyl group from the particle surface. It has been reported that presence of these hydroxyl and other ions (e.g., Cl^-) affects the crystallization, agglomeration and densification of fine ceramic powder [30]. The washed powders were oven dried for 24 h and a small part of the dried powder was subjected to thermal analysis in DSC/TG mode (Netzsch 402 C) till 1,200°C in air at a heating rate of 10°C/min. The dried powders were calcined in different temperature range from 650°C to 850°C/2 h. The phase analysis of the calcined powders was studied by XRD (Philips PW1830 Holland). The particle morphology was studied by TEM (Philiphs CM 200). The densification behaviour was studied in a dilatometer (Netzsch DL 402 C). The powders were uniaxially compressed at 280 MPa using PVA as binder. The density of the sintered samples were measured by Archimedes principle using kerosene as the immersion liquid. The strength of the sintered composites were measured in three point bending (span length = 20 mm) as well as diametral compression of the cylindrical disk (12.5 mm diameter). In order to study the effect of ZrO_2 addition in HA, pure HA powder was also synthesized by reverse strike method as described earlier and were similarly characterized.

3 Results and discussion

3.1 Thermal analysis

The DSC/TG curve of the precipitated powders of HA is shown in Fig. 2a. The curve shows a total weight loss of 5.78% which takes place in two stages, It has a broad but sharp endothermic peak in the temperature range 30–100°C with a peak at 70°C. This endothermic peak is associated with a weight loss of 3.55% which could be related to the loss of adsorbed water from hydroxyapatite. Following this peak, there is a broad and diffused exothermic peak in the temperature range 250–400°C. This exothermic peak also shows a gradual weight loss of about 2.23%. X-ray diffraction of the precipitated powder heated at 400°C shows peaks corresponding to HA only. Thus, this diffuse exothermic peak is due to the crystallization of HA from the precipitated amorphous powder.

Figure 2b shows the DSC/TG curve of the precipitated HA–2 wt% TZP powder. The nature of the curve and the total weight loss (4.74%) is comparable with that of pure HA (5.78%). This curve also shows one broad endothermic peak in the temperature range 30–100°C with peak at about 70°C along with a weight loss of 3.21% corresponding to the loss of adsorbed water. The weight loss is lower than pure HA as the amount of HA is less by 2%. Similarly, the second phase weight loss from 100°C to 400°C is also lower in HA–2 wt% TZP (HZ2) in comparison to pure HA. However, the exothermic peak of HZ2 is at a lower temperature as well it is relatively sharper in comparison to pure HA. This implies that the addition of ZrO_2 reduces the crystallization temperature and also improves the crystallization behaviour of HA. However, no further change in either the crystallization behaviour or the crystallization

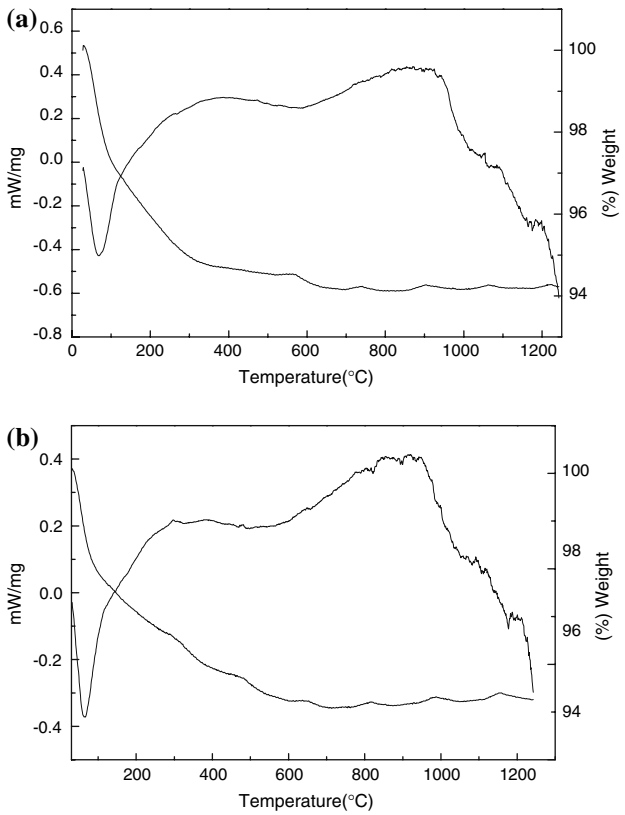

Fig. 2 Differential thermal analysis and thermo gravimetric curve of (**a**) HA powder; (**b**) curve of HZ2 powder

temperature could be observed in HA with still higher amount of zirconia (viz. HZ5, HZ7 and HZ10) samples.

3.2 FTIR

The FTIR spectra of pure uncalcined HA powder (Fig. 3) shows all the peaks corresponding to $(OH)^-$ and $(PO_4)^{-3}$ stretching and no extra peak could be observed. The broad peak between 3,750 cm^{-1} and 2,900 cm^{-1} corresponds to the hydrogen bonded O–H stretching of HA and water. In the calcined (850°C) HA powder, the presence of three strong peaks at around 1,060, 570 and 606 cm^{-1} relates to the P–O vibration modes [31]. The band at 570 and 606 cm^{-1} along with the band at 963 cm^{-1} corresponds to the bending mode of $(PO_4)^{3-}$ and the strong band at 1,060 cm^{-1} is due to the vibration of $(PO_4)^{3-}$ group [32]. It has been reported that the decomposition of HA to β-TCP causes a broadening of $(PO_4)^{-3}$ band at 1,060 and 960 cm^{-1} [33]. The absence of broadening of the peak at 1,060 cm^{-1} further confirms no decomposition of HA to β-TCP at 850°C. The increase in the sharpness of the peaks at 3,750 and 2,900 cm^{-1} with an increase in the calcination temperature indicates improved crystallization of HA and it also indicates an increase in the crystallite size of HA.

3.3 Phases and crystallite size of calcined powder

Figure 4 shows the XRD of calcined HA and different HA–TZP composite powder (HZ2, HZ5, HZ7, HZ10) at 850°C. The XRD pattern of the calcined powder shows only HA and t-ZrO_2 peaks are present. No other phases like β-TCP, $CaZrO_3$ or m-ZrO_2 could be detected. The intensity of t-ZrO_2 increases with the increase in zirconia content. Even at the highest calcination temperature (850°C), only HA and t-ZrO_2 could be detected. The intensity of the peaks increase and the peaks also became sharper with the increase in calcination temperature indicating that crystallite size increases on calcination at higher temperature. In the HZ10 composite the crystallite size of HA increased from 24.5 nm to 34.4 nm and that of ZrO_2 from 12.5 nm to 25.90 nm in the HA-TZP composites as the calcination temperature is increased from 650°C to 850°C.

3.4 Particle morphology of calcined powder

Figure 5a shows the dark field TEM photographs of HA calcined at 850°C. It could be seen that HA particles are mostly elongated although some cuboidal shaped particles are also seen in the size range 50–100 nm. Figure 5b shows that TEM photograph of HZ2 powder calcined at 850°C. The ZrO_2 parts which are mostly spherical shaped while the lighter ones are HA. It could also be seen from the micrographs that nano ZrO_2 (<50 nm) are uniformly distributed in the HA matrix.

3.5 Densification behaviour and phase analysis of sintered compacts

Figure 6a shows the nonisothermal densification behaviour of HA and HZ2, HZ5 and HZ10 green compacts up to 1,250°C. Except for HZ10, the densification of all other compacts started around 900°C. In HZ10 samples, the densification starts at around 1,000°C and densification has not reached the final stage at 1,250°C. Similarly in HZ7 samples, although the densification has started earlier (900°C), it did not reach the final stage till 1,250°C. This signifies that HZ7 and HZ10 sintering at higher temperature is required for complete densification. However, in HA, HZ2 samples, the

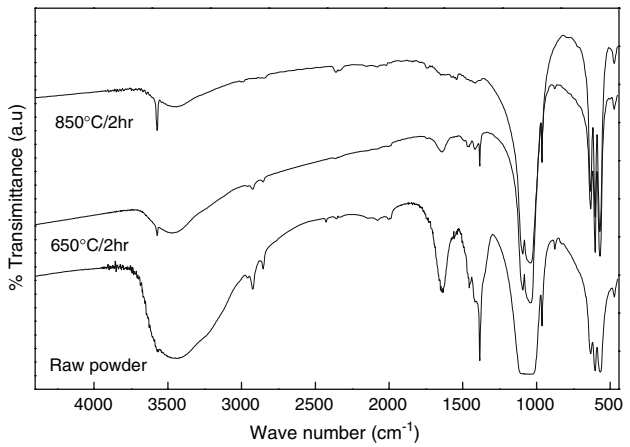

Fig. 3 FTIR Spectra of phase pure HA as a function of calcinations temperature

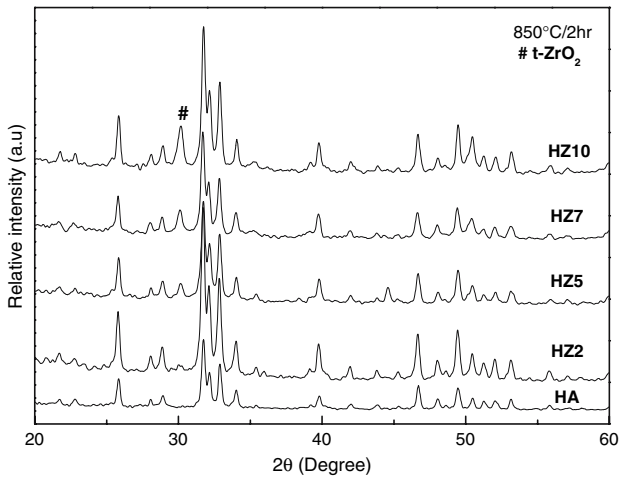

Fig. 4 XRD analysis of HA, HA–TZP (2, 5, 7.5, 10 wt%) powder calcined at 850°/2 h

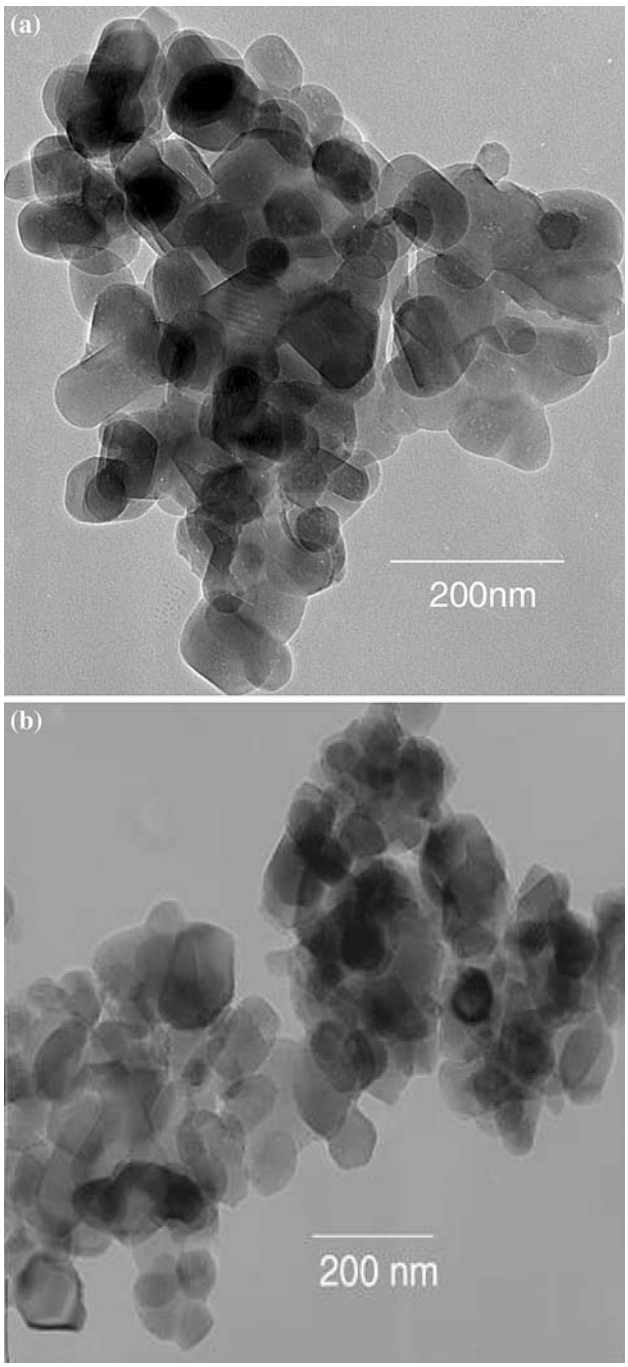

Fig. 5 (**a**) TEM of HA powder calcined at 850°/2 h. (**b**) TEM of HA–TZP (2 wt%) powder calcined at 850°/2 h

densification has reached the final stage and therefore, these two samples show high sintered density. The densification behaviour of HZ5 samples lie in between these two extremes and the slope change in densification curve at around 1,200°C shows that the final stage densification has started but the process is not complete and sintering at higher temperature would further densify HZ5 composites. These effects could be attributed to the addition of ZrO_2. With increasing ZrO_2 content, the densification shifts to a higher temperature. Further if the densification curve of HA and HZ2 are compared, it could be seen that although the shrinkage in HZ2 starts at higher temperature than HA, the shrinkage in HZ2 is more than HA and the densification is completed at a lower temperature than HA. Thus, HZ2, have a higher rate of densification and it can be assumed that ZrO_2 in this composition probably acts as a sintering aid. However this point need to further studied.

Figure 6b shows the plot of relative density versus sintering temperature for HA as well as HZ samples. The graph shows that for HA and HZ2 samples all the three stages of sintering (viz. initial, intermediate and final) could be clearly observed and in both of them the density has reached the plateau region. However, for HZ5 and HZ7, the final density has not been achieved at 1,250°C and the final stage density still has the rising trend. However, in HZ10 samples, the density graph could show only

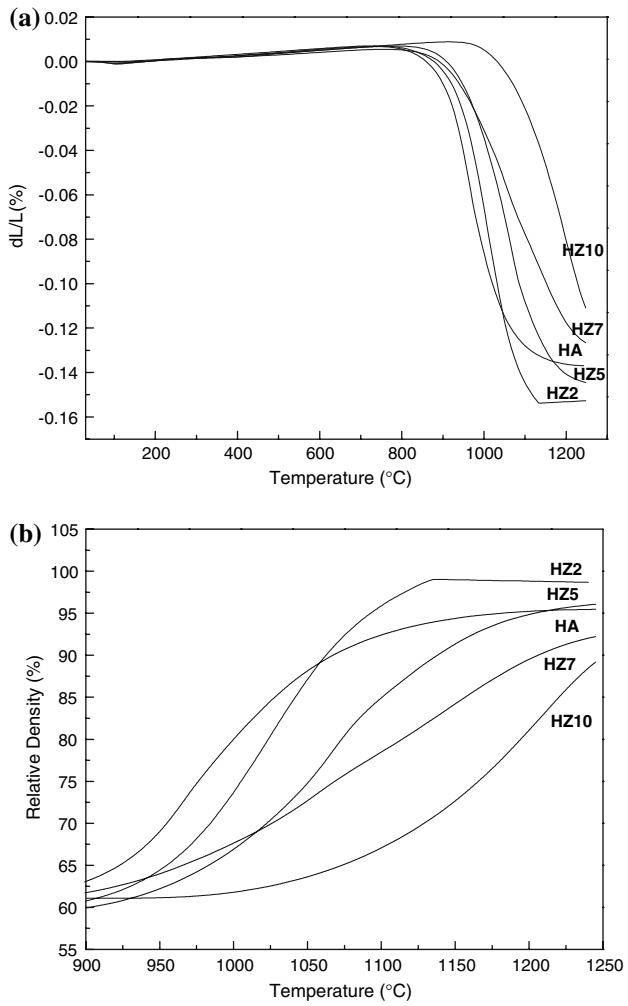

Fig. 6 (**a**) Non isothermal densification curve of HA, HA–TZP (2, 5, 7.5, 10 wt%). (**b**) Relative densities versus temperature profile with different zirconia content

the initial stage of densification and these samples would require further higher temperature to attain final density. This trend in densification is following the trend observed in other studied involving HA–TZP, where the retarded densification has observed with TZP addition. Pyda et al. [10] reported that the reduction in density of HA–ZrO_2 composites with increasing ZrO_2 content could be related to differential shrinkage of the two components (viz. HA and ZrO_2). By optimizing the calcination conditions this differential shrinkage could be reduced which is expected to give higher sintered density of the composites.

Figure 7 shows the XRD pattern of the sintered samples of HA and HZ2 to HZ10. It is observed that HA is stable till 1,250°C and no other phases (e.g., β-TCP, $CaZrO_3$) could be detected. Similarly in HZ2 samples, only HA and t-ZrO_2 could be detected and identified. However, in HZ5 and HZ7 samples, beside HA and t-ZrO_2, small amount of $CaZrO_3$ ($d = 2.84$ A°) and β-TCP ($d = 2.90$ Å) could also be seen. $CaZrO_3$ and β-TCP probably formed according to the reactions given below:

$$\text{t-}ZrO_2 + CaO \rightarrow CaZrO_3 \quad (1)$$

$$Ca_{10}(PO_4)_6(OH)_2 \rightarrow 3Ca_3(PO_4)_2 + CaO + H_2O \quad (2)$$

Thus, retained HA in HZ5 may be a little Ca-deficient. Further a small peak of β-TCP was also identified in HZ10 samples. However, no $CaZrO_3$ peak was detected in HZ10 samples. Thus it is seen that progressive addition of TZP to HA, results in partial decomposition of HA to $CaZrO_3$ and/or TCP phase along with substantial fraction of retained t-ZrO_2 and HA.

3.6 Mechanical properties

Figure 8a shows the variation of three point bending strength of HA and HA–TZP sintered composites (HZ2, HZ5, HZ7 and HZ10) as a function of TZP content. The curve shows that pure HA has bending strength of about 35 MPa which increases sharply to 70 MPa at 2 wt% TZP addition. Following this, the bending strength drops to about 30 MPa for HZ5. It further increases to about 40 MPa for HZ7 and there after the drop in strength is very less for HZ10 (37 MPa). The sintered density on the other hand increases for HZ2 and it decreases gradually with further addition of TZP. Similar trend in strength and density value is observed for diametral compression strength as shown in Fig. 8b. The strength and density variation does not follow the well known relation $\sigma = \sigma_0 \exp(-bp)$. This drop in strength for HZ5 to HZ10 samples could be attributed to the residual porosity present due to incomplete sintering.

3.7 Microstructure of sintered HA–ZrO_2 composites

The microstructure of the sintered HA–ZrO_2 composites was observed in SEM (JEOL, JSM-6480 LV). The sintered

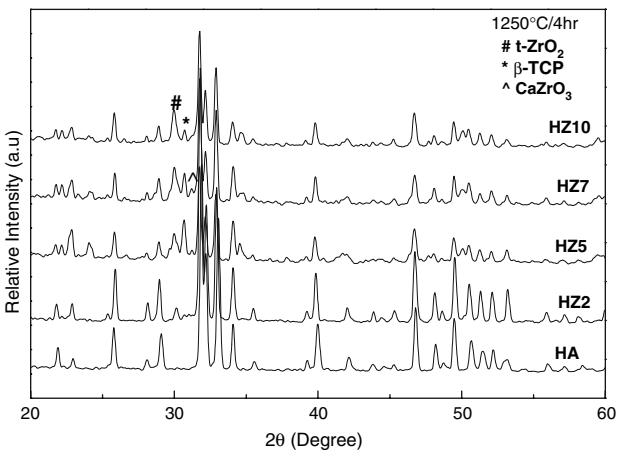

Fig. 7 XRD analysis of HA, HA–TZP (2, 5, 7.5, 10 wt%) compacts sintered at 1,250°C/4 h

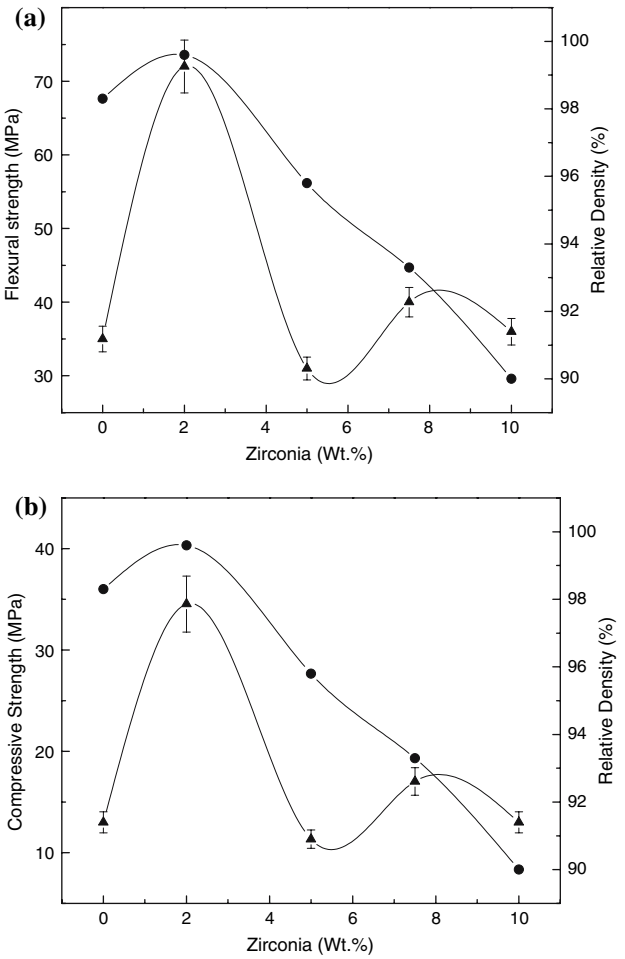

Fig. 8 (**a**) Flexural strength as a function of zirconia content. (**b**) Compressive strength as a function of zirconia content

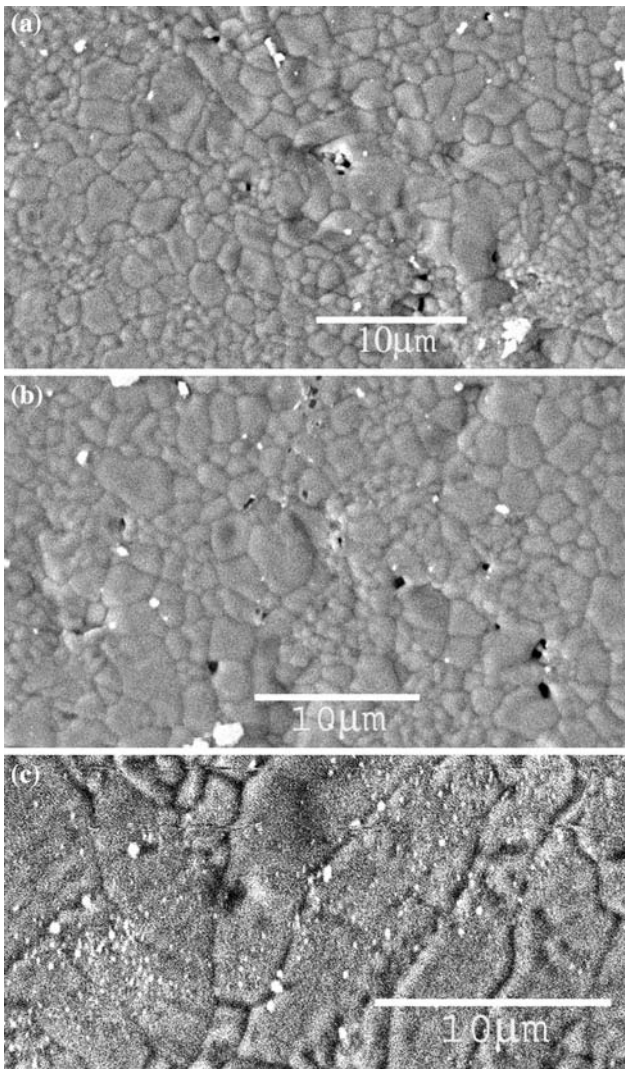

Fig. 9 SEM of HA, HA–ZrO_2 composites sintered at 1,250°C/4 h (**a**) HZ5, (**b**) HZ7, (**c**) HZ10

sample were lightly polished on a velvet cloth, cleaned and thermally etched at 1,100°C for 20 min. Figure 9a–c shows the microstructure of sintered compacts of HZ5, HZ7, HZ10 in BSE mode. Due to very small amount of ZrO_2 in HZ2, the ZrO_2 distribution could not be properly observed. The bright spots are ZrO_2 while that of HA grains are darker. The grain size of HA changes on increasing ZrO_2 content. This is in agreement with literature [10, 17], because ZrO_2 addition affects grain growth of HA. But it is also noted that except for a few clusters, ZrO_2 has a nearly uniform dispersion. Even at the highest vol% of ZrO_2 (HZ10), the dispersion is very uniform and nano ZrO_2 could be seen dispersed in HA. However, it should also be mentioned that although a good dispersion of ZrO_2 could be achieved, compositions containing higher ZrO_2 amount could not be sintered to near theoretical density. This causes a reduction in strength at higher ZrO_2 addition.

4 Conclusions

HA–TZP containing varying amount of TZP (2, 5, 7.5 and 10 wt%) were prepared by reverse strike precipitation method. The powders crystallized around 400°C. While pure HA was mostly elongated, addition of TZP partially changed the morphology to cuboidal/spherical shape also. The calcined samples of all the composition had only HA and t-ZrO_2. Sintering at 1,250°C also produced β-TCP and trace amount $CaZrO_3$ along with HA and t-ZrO_2 for HZ5 and HZ7 samples while in HZ10 β-TCP, HA and t-ZrO_2 was present. The densification rate increases for HZ2 samples which indicate that at that composition TZP may be acting as a sintering aid. ZrO_2 was dispersed uniformly. The decrease in strength could be related to residual porosity.

References

1. L.L. Hench, J. Am. Ceram. Soc. **81**, 1705 (1998)
2. L.L. Hench, J. Wilson, Science. **226**, 630 (1984)
3. G. De With, H.J.A. Van Dijk, N. Hattu, K. Prijs, J. Mater. Sci. **16**, 1592 (1981)
4. K. Ioku, S. Somiya, M. Yoshimura, J. Ceram. Soc. Jpn. Int. Ed. **99**, 191 (1991)
5. M. Knepper, B. Milthrop, S. Moricca, J. Mater. Sci. Mater. Med. **9**, 589 (1998)
6. Y.-M. Kong, S. Kim, H.-E. Kim, J. Am. Ceram. Soc. **82**, 2963 (1999)
7. Z. Shen, E. Adolfsson, M. Nygren, L. Gao, H. Kawaoka, K. Niihara, Adv. Mater. **13**, 214 (2001)
8. H.-W. Kim, Y.-H. Koh, B.-H. Yoon, H.-E. Kim, J. Am. Ceram. Soc. **85**, 634 (2002)
9. V.V. Silva, F.S. Lameiras, Mater. Charact. **45**, 51 (2000)
10. W. Pyda, A. Slosarczyk, M. Haberko, Z. Paszkiewicz, A.R. Kmita, A. Pyda, Key Eng. Mater. **206**, 1567 (2002)
11. E.S. Ahn, N.J. Gleason, J.Y. Ying, J. Am. Ceram. Soc. **88**, 3374 (2005)
12. N. Thangamani, K. Chinnakalib, F.D. Gnanam, Ceram. Int. **28**, 355 (2002)
13. S.J. Kalita, S. Bose H.L. Hosick, A. Bandyopadhyay, Biomaterials. **25**, 2331 (2005)
14. J. Li, L. Hermansson, R. Soremark, J. Mater. Sci.: Mater. Med. **4**, 50 (1993)
15. D.K. Pattanayak, R. Dash, R.C. Prasad, B.T. Rao, T.R. Rama Mohan, Mater. Sci. Eng. C, doi:10.1016/j.msec.2006.06.021
16. S. Meejoo, W. Maneeprakorn, P. Winotai, Thermochim. Acta. **447**, 115 (2006)
17. J.M. Wu, T.S. Yeh, J. Mater. Sci. **23**, 3771 (1988)
18. M.S. Kaliszewski, A.H. Heuer, J. Am. Ceram. Soc. **73**, 1504 (1990)
19. N.Y. Mostafa, Mater. Chem. Phys. **94**, 333 (2005)
20. J. Li, H. Liao, L. Hermansson, Biomaterials **17**, 1787 (1996)
21. D.C. Tancred, A.J. Carr, B.A.O. McCormack, J. Mater. Sci: Mater. Med. **12**, 81 (2001)
22. B.K. Moon, D.H. Choi, R.J. Sung, S.H. Kim, K. Niihara, Mater. Sci. Forum. **486**, 101 (2005)
23. X. Miao, Y. Chen, H. Guo, K.A. Khor, Ceram. Int. **30**, 1793 (2004)
24. H.W. Kim, Y.J. Noh, Y.H. Koh, H.E. Kim, H.M. Kim, Biomaterials **23**, 4113 (2002)

25. N. Kawashima, K. Soetanto, K.I. Watanabe, K. Ono, T. Matsuno, Colloid. Surface. B: Bioint. **10**, 23 (1997)
26. R. Kumar, K.H. Prakash, P. Cheang, K.A. Khor, Acta Materialia. **53**, 2327 (2005)
27. W. Pyda, A. Slosarczyk, Z. Paszkiewicz, A.R. Kmita, M. Haberko, A. Pyda, Mater. Sci. Forum. **492**, 241 (2005)
28. Z. Evis, R.H. Doremus, Scripta Materialia. **56**, 53 (2007)
29. A.R. Kmita, A.S. lo sarczyk, Z. Paszkiewicz, C. Paluszkiewicz, J. Mol. Struct. **704**, 340 (2004)
30. R.P. Rana, S.K. Pratihar, S. Bhattacharyya, J. Mater. Sci. **41**, 7025 (2006)
31. Y. Sun, G. Guo, Z. Wang, H. Guo, Ceram. Int. **32**, 951 (2006)
32. R. Murugan, S. Ramakrishna, Mater. Lett. **58**, 230 (2003)
33. S. Meejoo, W. Maneeprakorn, P. Winotai, Thermochim. Acta. **447**, 115 (2006)